

Ion Transporter NKCC1, Modulator of Neurogenesis in Murine Olfactory Neurons*

Received for publication, January 27, 2015, and in revised form, February 10, 2015. Published, JBC Papers in Press, February 20, 2015, DOI 10.1074/jbc.M115.640656

Claudia Haering^{†1}, Ninthujah Kanageswaran[‡], Pascal Bouvain[‡], Paul Scholz[‡], Janine Altmüller[§], Christian Becker[§], Günter Gisselmann[‡], Janine Wäring-Bischof[‡], and Hanns Hatt[‡]

From [†]Cell Physiology, Ruhr-University Bochum, Universitätsstr. 150, 44780 Bochum, Germany and the [§]University of Köln, Cologne Center for Genomics, Köln, Germany

Background: NKCC1 is controversially discussed as the main chloride transporter in olfactory epithelium.

Results: Lack of NKCC1 results in impaired odorant detection and a decrease in the number of mature neurons.

Conclusion: NKCC1 is involved in chloride accumulation but also reveals an impact in neurogenesis.

Significance: This work contributes to the understanding of olfactory epithelium neurogenesis.

Olfaction is one of the most crucial senses for vertebrates regarding foraging and social behavior. Therefore, it is of particular interest to investigate the sense of smell, its function on a molecular level, the signaling proteins involved in the process and the mechanism of required ion transport. In recent years, the precise role of the ion transporter NKCC1 in olfactory sensory neuron (OSN) chloride accumulation has been a controversial subject. NKCC1 is expressed in OSNs and is involved in chloride accumulation of dissociated neurons, but it had not been shown to play a role in mouse odorant sensation. Here, we present electro-olfactogram recordings (EOG) demonstrating that NKCC1-deficient mice exhibit significant defects in perception of a complex odorant mixture (Henkel100) in both air-phase and submerged approaches. Using next generation sequencing (NGS) and RT-PCR experiments of NKCC1-deficient and wild type mouse transcriptomes, we confirmed the absence of a highly expressed ion transporter that could compensate for NKCC1. Additional histological investigations demonstrated a reduced number of cells in the olfactory epithelium (OE), resulting in a thinner neuronal layer. Therefore, we conclude that NKCC1 is an important transporter involved in chloride ion accumulation in the olfactory epithelium, but it is also involved in OSN neurogenesis.

The primary odorant perception of vertebrates occurs in the cilia of the olfactory sensory neuron (OSN).² In the majority of the OSNs, odorant recognition is primarily mediated through a

cAMP-dependent signaling pathway. This pathway's mechanism has been well characterized, while some of the ion transporters and channels involved remain unclear. First, odorant recognition is initiated by odorant molecule binding to its specific G protein-coupled receptor. Through G protein activation, the α subunit binds to adenylyl cyclase, which catalyzes cyclic adenosine monophosphate (cAMP) formation (1, 2). Subsequently, the increased cAMP concentration induces cyclic nucleotide-gated channel opening, thereby inducing an influx of calcium ions and initializing OSN depolarization (3). Calcium ion binding to a calcium-activated chloride channel leads to its opening and a subsequent efflux of chloride ions due to the high chloride level in OSNs (4–6). This chloride efflux represents the primary depolarization (80%) of an olfactory neuron (7). In conclusion, olfactory epithelium neurons require the active accumulation of chloride ions, namely by a chloride ion transporter.

The identity of the chloride transporter responsible for OSN chloride accumulation has remained unclear for years. One potential candidate is the Slc12 transporter family member NKCC1, which is a sodium-, potassium-, and chloride-symporter that electroneutrally transports 1 Na⁺, 1 K⁺, and 2 Cl⁻ ions (8). NKCC1 is widely distributed throughout the entire human body and in different cell types, where it functions as a chloride accumulator. For example, it functions in colonic epithelial cells, the cochlear exocrine glands, neurons in the brain and in trigeminal ganglion neurons (9–12). The NKCC1 transporter is highly expressed in the brain, and its expression decreases during development (13). This change in chloride concentrations alters GABA-induced responses in neurons, and thus, is thought to play a major role in the plasticity of the brain (14, 15). NKCC1 is also expressed in the OE, and it affects chloride accumulation in acute dissociated olfactory neurons. Loss of NKCC1 has been shown to affect electro-olfactogram recordings (EOGs) of intact olfactory tissue (16, 17). It has previously been shown that mice lacking the ion transporter exhibit a 39 or 57% reduction in generated amplitudes in EOGs compared to wild type mice, depending on the study (17, 18). In contrast, behavioral tests of mice lacking the transporter showed no impairment in odorant perception (19). These con-

* This work was supported by the SFB 642, the International Max Planck Research School in Chemical and Molecular Biology (IMPRS-CMB), and the Ruhr-University Bochum Research School.

The raw RNA-Seq data sets (FASTQ file format) for OE of wild type and NKCC1-deficient mice were deposited in Gene Expression Omnibus (GEO) repository (www.ncbi.nlm.nih.gov/geo/) under the following accession number: GSE65388.

¹ To whom correspondence should be addressed: Cell Physiology, Ruhr-University Bochum, Universitätsstr.150, 44780 Bochum, Germany. Tel.: 49-234-32-28841; Fax: 49-234-14129; E-mail: Claudia.Haering@rub.de.

² The abbreviations used are: OSN, olfactory sensory neurons; NKCC1, Na-K-Cl cotransporter; OE, olfactory epithelium; EOG, electro-olfactogram recordings; KO, knockout; cAMP, cyclic adenosine monophosphate; FPKM, fragments per kb of exon per million fragments mapped; FACS, fluorescence-activated cell sorting.

Ion Transporter Composition of the Murine Olfactory Epithelium

controversial findings require further investigations into the role of NKCC1 in OSN function.

In addition to its ion accumulation function, NKCC1 plays a major role in cell proliferation of cultured cell lines. NKCC1 regulates the resting phase and early interphase (G1) of the cell cycle in mouse fibroblasts. Upon NKCC1 overexpression, proliferation is induced, and mouse fibroblasts undergo phenotypic transformation (20, 21). Conversely, treatment of the PC12D rat pheochromocytoma cell line with nerve growth factor induces NKCC1 up-regulation, demonstrating the relationship between neurite outgrowth and NKCC1 expression (22). NKCC1 also contributes to cell regeneration after both nerve injury in dorsal root ganglia and traumatic brain injury (23, 24). Moreover, pharmacological NKCC1 inhibition reduces the proliferation of forebrain neuronal progenitor cells. These results suggest that NKCC1 may regulate postnatal neurogenesis (25). Although several studies indicate the involvement of NKCC1 in cell proliferation of numerous cell types, its impact on olfactory neurogenesis has not been studied.

Here, we demonstrate that loss of NKCC1 in mice results in significant defects in olfactory perception and has additional impacts on olfactory epithelium morphology. Thus, the ion transporter NKCC1 is involved in chloride accumulation and has an important influence on the continuous neurogenesis of the murine olfactory epithelium.

EXPERIMENTAL PROCEDURES

Animals—NKCC1-deficient mice were generated by Prof. Dr. Gary Shull, University of Cincinnati and kindly provided by Prof. Dr. med. Ursula Seidler, University of Hannover (26). Genotyping was performed using the Phire[®] Animal Tissue Direct PCR kit (Finnzyme, Finland) according to the instruction manual. Primers for the wild type gene were: NKCC1-for: 5'-GGA ACA TTC CAT ACT TAT GAT AGA TG-3' and NKCC1 rev: 5'-CTC ACC TTT GCT TCC CAC TCC ATT CC-3' (fragment size: 105 bp). Primers for the mutant gene were: NKCC1-for and dNEO-Poly(A): 5'-GAC AAT AGC AGG CAT GCT GG-3' (fragment size: 156 bp) (26). Mice were offered normal laboratory chow and water *ad libitum* in standard cages. All animal experiments were performed in accordance with the European Union Community Council guidelines and approved by the competent state office of the Federal Land of Northrhine Westphalia (file number 87-51.04.2010.A180).

RNA-Seq: Preparation of Mice OE—OE from male and female NKCC1^{+/+} (12 ± 1 week) and NKCC1^{-/-} mice (16.5 ± 3.5 weeks, NMRI background) was prepared, and RNA was isolated; total RNA was prepared from an OE pool of 4 (mixed-gender pool RNA isolation) or 2 (gender RNA pool) different mice for each condition.

RNA Isolation—Total RNA was isolated with the RNeasy Plus Mini Kit (Qiagen, Hilden, Germany) according to the manufacturer's protocol including the optional on-column DNaseI digestion.

NGS Library Preparation and Illumina Sequencing—Libraries for NGS sequencing were prepared from total RNA and subjected to DSN normalization by standard Illumina protocols. Afterward, Illumina sequencing was performed on a HiSeq 2000 by standard Illumina protocols (101-bp, paired-end).

Alignment of RNA-Seq Reads using TopHat—We analyzed the raw sequence data in fastq format as previously described (27). RNA-Seq reads were aligned to version mm9 of mouse reference genome and transcriptome using TopHat (v2.0.7) (28), which utilizes the ultra-fast short-read mapping program Bowtie to arrange the alignment (29). TopHat output files in BAM format were sorted and indexed with SAMtools (30). To reduce the alignment of repetitive reads a multiread-correction was used allowing up to 5 hits per read.

Gene Expression Calculation using Cufflinks—Aligned RNA-Seq reads for each sample were assembled into transcripts and their abundance was estimated by the program Cufflinks (v1.3.3) (31) using the RefSeq mm9 reference transcriptome in Gene Transfer Format (GTF) obtained from the UCSC Genome Bioinformatics database (University of California, Santa Cruz Biotechnology). To estimate transcript expression, the GTF-file was supplied to Cufflinks. The parameter `-compatible-hits-norm` was set to ensure that FPKM normalization was performed based on reference transcriptome only. Cufflinks was provided with a multifasta file (mm9.fa) to improve accuracy of the relatively transcript abundance estimation (32). We further used a masked command `-M` and the mask GTF `rmsk.gtf` to mask all possible reads from RNA repeats (including tRNA, snRNA, scRNA, srpRNA) short and long interspersed nuclear elements (SINE, LINE) and other classes of repeats. Cufflinks indicates and quantifies the relative abundances of transcripts in the unit FPKM (31). The data sets were visualized and investigated by the Integrative Genomics Viewer (www.broadinstitute.org/igv) for proving sequence alignments and correct mapping of reads for the top expressed genes. While the raw data analysis was performed on a Linux based computer further calculations were carried out with Microsoft Excel 2010. For a differential gene expression analysis, we used the program Cuffdiff, which identifies significant changes in transcript expression between two datasets (27).

Availability of Raw Data Sets—The raw RNA-Seq data sets (FASTQ file format) for OE of wild type and NKCC1-deficient mice were deposited in Gene Expression Omnibus (GEO) repository (www.ncbi.nlm.nih.gov/geo/) under the following accession number: GSE65388.

Reverse Transcriptase (RT)-PCR—Adult mice (over 3 months old) of each genotype (NKCC1^{+/+} and NKCC1^{-/-}) were sacrificed by cervical dislocation and subsequently decapitated. OE was carefully collected to prevent olfactory bulb tissue contamination. RNA purification was performed with the RNeasy Mini kit (Qiagen, Hilden, Germany), and cDNA was prepared with the iScript[™] cDNA Synthesis kit (BioRad). Primers were typically 22-bp long and designed to generate a 153–404 bp DNA fragment. To avoid gDNA detection and false-positive amplification, primers were designed to bind to an exon-exon junction. RT-PCR was performed with iQ[™] SYBR[®] Green Supermix in an Eppendorf Mastercycler[®] realplex2 real-time PCR machine (Eppendorf, Hamburg, Germany) whereby each approach was divided for triple determination of CT-values (40 cycles: 50–60 °C for 45 s, 72 °C for 1 min, 95 °C for 45 s). PCR products were analyzed on a 1% agarose gel. Control experiments were performed with a -RT (no-reverse transcriptase) template or water.

Electro-olfactogram Recordings—EOGs were recorded on olfactory epithelia located on the septum of adult NKCC1^{+/+}, NKCC1^{+/-}, and NKCC1^{-/-} in an inbred NMRI background according to previously described methods (33). The head was flayed and sagittally hemisected to expose the septum, which is covered with OE. The halved head was placed on an agarose block in which the reference electrode was embedded. Additionally, the Ag/AgCl recording electrode filled with Ringer solution was placed directly on the epithelium surface, exemplified by the increase in electrical resistance. The electro-olfactogram recordings were performed while a continuous humidified air stream (2.4 liter/min) was applied to the OE on the septum. Provoking a change in the surface potential, an odorant mixture of 100 odorants [Henkel100 (Henkel, Düsseldorf, Germany), 1:1000 dilution in Ringer] was delivered for 100 ms on the OE, which was injected into the air stream via a custom-made device. Ringer solution: 140 mM NaCl, 5 mM KCl, 2 mM CaCl₂, 2 mM MgCl₂, 10 mM HEPES pH 7.4. Surface potentials were generated at 10 different OE locations, and in the case of dose-dependent stimulation, at three different locations. Responses were recorded, and the average amplitude and area under curve were calculated for each mouse. Student's *t* test was used for statistical analysis, and significant differences were calculated (***: *p* < 0.001; **: *p* < 0.01; *: *p* < 0.05). In addition, rise and decay time were calculated via curve fitting with Igor Pro software (version 6.0).

Submerged Electro-olfactogram Recordings—The OE was exposed as described. In addition, the halved head was placed in low melting agarose to facilitate a transverse position of the septum. The OE was continuously perfused with oxygenated saline (95% O₂, 5% CO₂) using a custom-made air-pressure application device (0.6 ml/min) whereby the application cannula was placed on the calvaria. Oxygenated saline buffer: 120 mM NaCl, 25 mM NaHCO₃, 5 mM KCl, 5 mM BES, 1 mM MgSO₄, 1 mM CaCl₂, and 10 mM glucose, pH 7.5. The continuous stream of buffer solution was ensured by using a suction cannula located under the septum edge. The recording pipette tip (2 MΩ) was first soaked with 3% agarose, filled with Ringer solution and placed on the OE surface before continuous oxygenated saline application. In addition, the reference electrode was embedded in the low melting agarose. OE stimulation was computer-controlled (0.5 s), which allowed for rapid and consistent application of the odorant mixture Henkel100. For blocking experiments, 300 mM niflumic acid was applied for 20 s and washed out with Ringer solution for 5 min. Surface potentials were recorded and amplified with a DigiData 1200 Series interface (WPI), a 5111A oscilloscope (Tektronix) and DP-311 differential amplifier and visualized with the WinEDR V.3.1.2. program (University of Strathclyde, Glasgow, Scotland). Student's *t* test was used for statistical analysis of the amplitude, and significant differences were calculated (***: *p* < 0.001; **: *p* < 0.01; *: *p* < 0.05).

Western Blot Analysis—Protein content of specific signal transduction proteins in the wild type and NKCC1-deficient OE was analyzed by Western blotting. Epithelium preparation was performed as described previously, collected in RIPA buffer (150 mM NaCl, 50 mM Tris-HCl, 1% Nonidet, 0.5% sodium deoxycholate (*w/v*), 0.1% SDS (*w/v*), pH 7.5, and prote-

ase inhibitors) and mechanically solubilized. Cell lysate was loaded onto an SDS gel, and immunoblotting was executed (Porablot NCL nitrocellulose membrane, Machery-Nagel). The presence of protein was detected with specific antibodies (dilution 1:50–2,500) and a chemiluminescence detection system (GE Healthcare).

Antibodies—The primary antibodies used were as follows: NKCC1 (rabbit polyclonal, catalogue number ab59791, Abcam), Gα_{olf} (mouse monoclonal, catalogue number sc55545, Santa Cruz Biotechnology) calmodulin (mouse monoclonal, catalogue number sc-137079, Santa Cruz Biotechnology), CNGA2 (goat polyclonal, catalogue number sc-13700), adenylyl cyclase III (rabbit polyclonal, catalogue number sc-588), phosphodiesterase (PDE1C, rabbit polyclonal, catalogue number sc-67323, Santa Cruz Biotechnology), acetylated α-tubulin (mouse monoclonal, catalogue number sc-23950, Santa Cruz Biotechnology) and β-actin (rabbit polyclonal, catalogue number ab-8227, Abcam). Secondary antibodies were horseradish peroxidase (HRP)-coupled goat anti-mouse, donkey anti-goat, and goat anti-rabbit IgGs (1:10,000) (Bio-Rad), and goat anti-rabbit or -mouse and rabbit anti-goat IgG conjugated to Alexa Fluor 488 (Molecular Probes).

Measurement of Neuronal Layer Thickness and Turbinate Length and Cell Counting—OE cryosections (14 μm) were prepared as described previously (34). In addition, the tissue was stained with hematoxylin and eosin (Sigma-Aldrich) and subsequently analyzed by microscopy (Zeiss Axio Scope). Three different cryosections were analyzed for each mouse whereby images of the olfactory neuronal layer were acquired with a 40-fold magnification in the same area of the nasal cavity. Neuronal layer thickness was measured 5 times in each nasal cavity using Java-based ImageJ 1.46 for analysis (35). Moreover, cells located in the OE neuronal layer were counted using a DAPI stain. Therefore, three cryosections of each mouse were stained with DAPI and analyzed with a Zeiss LSM 510 Meta confocal microscope using a 40-fold magnification. Cell counting was performed in ImageJ whereby the cell number was normalized to the neuronal layer area. To obtain turbinate length, images of the halved head were acquired. For individual distance calibration, the head was placed on graph paper. The distance between the tip of the nose and the olfactory bulb for each mouse was measured and used for normalization of the turbinate length using ImageJ for analysis.

RESULTS

RNA-Seq of NKCC1^{-/-} versus NKCC1^{+/+}—To characterize transporter gene expression in NKCC1^{-/-} mice, we examined the OE gene profile (Fig. 1) using Illumina RNA-Seq to generate OE transcriptomes from NKCC1^{-/-} and NKCC1^{+/+} (wild type) mice. We prepared three OE samples for each condition (wild type/NKCC1^{-/-}), one sample of mixed gender and two additional samples of male only and female only. Each RNA sample was prepared from the OE of three different mice; in the mixed gender pool, we used two OE of each gender. In total, we amplified and sequenced up to 38 million 101-nt long fragments from NKCC1^{+/+} and NKCC1^{-/-} adult mouse OEs (Fig. 1A). We analyzed our sequencing results using TopHat and Cufflinks software (27),

Ion Transporter Composition of the Murine Olfactory Epithelium

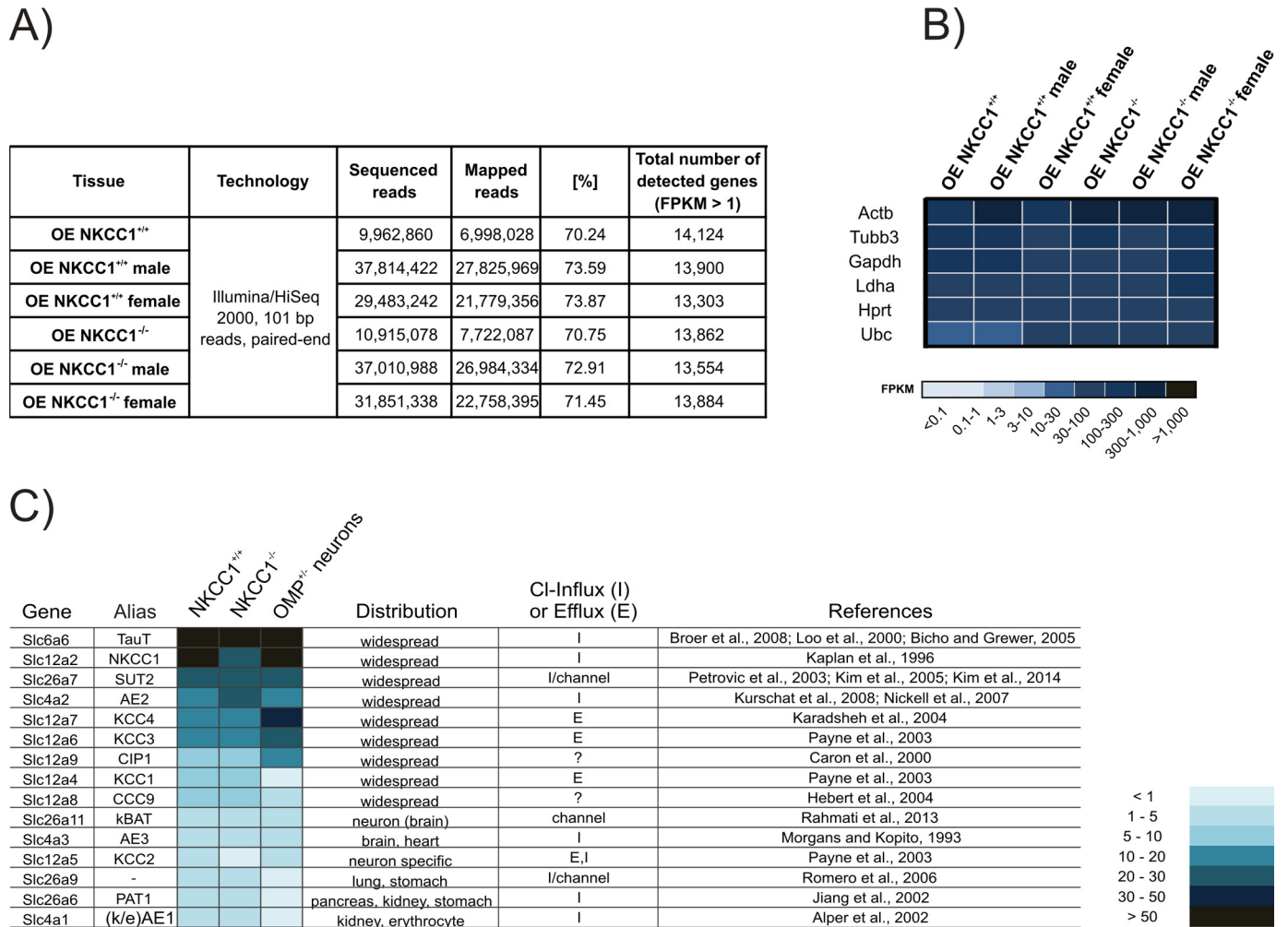


FIGURE 1. Summary of RNA-Seq data. *A*, list of generated and mapped reads for each RNA-Seq analysis of different OE pools. *B*, distribution of different housekeeping genes in OE samples of NKCC1^{-/-}-deficient and WT mice. Heatmap showing the expression levels of different housekeeping genes in OE samples of wild type (mixed gender, male, and female OE sample). Higher FPKM values are indicated by darker colors. *Actb*: actin, cytoplasmic 1, *Tubb3*: tubulin β -3 chain, *Gapdh*: glyceraldehyde-3-phosphate dehydrogenase, *Ldha*: L-lactate dehydrogenase A chain isoform, *Hprt*: hypoxanthine-guanine phosphoribosyltransferase 2, *Ubc*: polyubiquitin-C. *C*, Next Generation Sequencing results for putative chloride-related and anion/cation organic transporters of the olfactory epithelium with FPKM averages over 1 ($n = 3$). Transporter families: Slc4 and Slc26 belong to anion exchangers, Slc6: sodium-/chloride-dependent neurotransmitter and amino acids transporter, Slc12: electroneutral, cation-coupled cotransporters, Slc14/Slc22: organic anion/cation transporters.

and reads were mapped to the mouse reference genome mm9. We calculated expression values from the number of reads per kilobase per million reads in each sample. The quantitative measurement of gene expression employed in the RNA-Seq experiments was the FPKM (fragments per kilobase of exon per million fragments mapped) value. Our analysis enabled us to detect up to 14,124 genes in wild type/NKCC1-deficient mice (FPKM > 1) of the 22,310 genes interrogated with a Refseq-based gene model. Including genes with an extremely low expression level (FPKM < 1), we counted an additional 3,481 genes. For differential gene expression analysis between wild type and NKCC1-deficient mice, we analyzed the three OE transcriptome raw datasets for each condition (wild type/NKCC1-deficient) in Cuffdiff (27) (Fig. 1A). To ensure the comparability of datasets, we studied expression patterns of different housekeeping genes (Fig. 1B). A general rough scale regards FPKM values ~1 to indicate weakly expressed genes, ~10 indicates medium expression, and ~100 indicates highly expressed genes based on comparisons to housekeeping genes. Addition-

ally, we used published RNA-Seq data from olfactory marker protein (OMP) heterozygous FACS-sorted OSNs (34), which enabled us to compare these data with the results of OE tissue from wild type and NKCC1-deficient mice.

Chloride-associated Cotransporters—The OE consists of different cell types with distinct functions, including the olfactory neurons, the supporting cells and the basal cells (36, 37). We first screened the OE expression level of several chloride-related ion transporters that had a FPKM higher than 1 in wild type mice and have been previously described in literature (17) (Fig. 1C). Because our data referred to the whole OE transcriptome, we compared our results to previously published RNA-Seq data of fluorescence-activated cell sorted (FACS) heterozygous OMP-GFP neurons (34). Comparing both data sets, we identified transporters primarily expressed in ORNs or other OE cell types. We identified 15 Slc-transporters whereby 9 showed a low expression profile in wild type (FPKM: 1–10), 4 displayed medium expression (FPKM: 10–50) and 2 demonstrated high expression (FPKM > 50). The RNA-Seq results

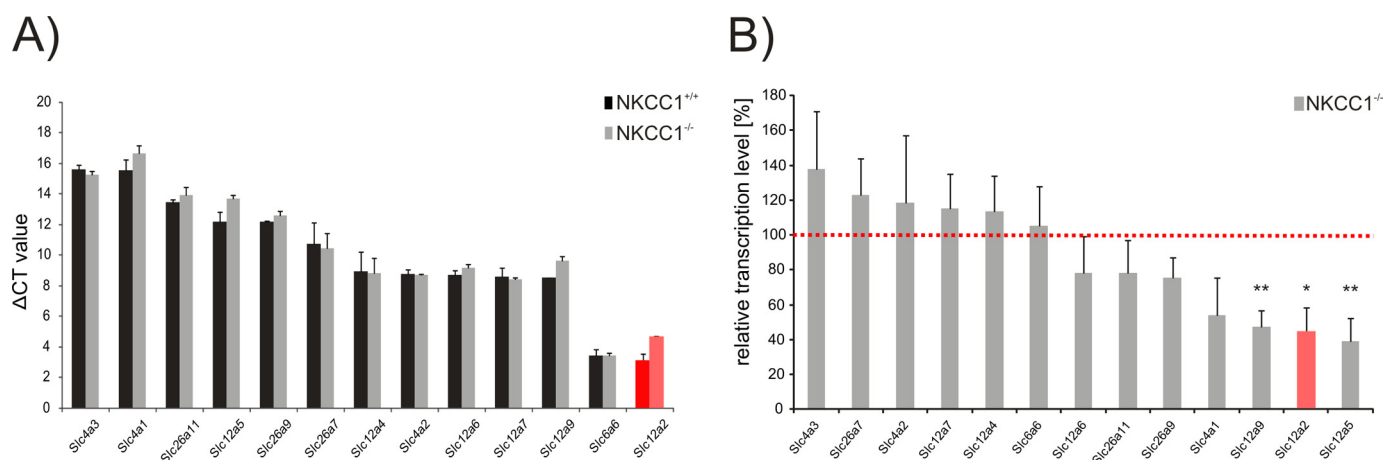


FIGURE 2. **Transcription level of chloride-related ion transporters.** *A*, Δ CT values of ion transporters of olfactory epithelium. Values are normalized to β -actin expression. *B*, relative mRNA transcription level of transporters found in NKCC1-deficient OE compared with wild type (100%, indicated by red dotted line). Slc12a2 corresponds to NKCC1 ($n = 3$).

revealed high mRNA transcription of the Slc6a6 transporter in wild type (FPKM: 85.2), NKCC1-deficient OE (84.6) and FACS-sorted heterozygous OMP-GFP neurons (71.9) (38). Interestingly, Slc12a2, which encodes the protein NKCC1, displayed the second highest FPKM in wild type OE (FPKM: 50.7). FACS-sorted heterozygous OMP-GFP neurons also demonstrate the outstanding FPKM value for NKCC1 (FPKM 188), which was 2.6 times higher than Slc6a6. In addition, we detected NKCC1 mRNA in knock-out mouse OE due to the nature of the mouse. The neomycin cassette was inserted into exon 6 of the NKCC1 gene to disrupt the reading frame. Therefore, mRNA of the NKCC1 gene is expressed resulting in a nonfunctional protein, which is degraded in deficient mice (Fig. 3B). The FPKM value (20.7) assigned for the NKCC1 gene was less than half of the wild type value (50.7). The third highest expressed transporter was the Slc26a7 anion exchanger. This transporter exhibited a constant expression pattern with an average FPKM of 26 in the three transcriptome pools. A slightly lower FPKM value was obtained for the Slc4a2 anion exchanger in NKCC1-deficient (25.9) and wild type OE (19.7). The cation-coupled cotransporter members 6 and 7 demonstrated uniform expression in both wild type and NKCC1-deficient OE. We verified the RNA-Seq results with RT-PCR and obtained similar expression levels (Fig. 2A). The RT-PCR results confirmed that the taurin transporter TauT (Slc6a6) and NKCC1 (Slc12a2) were most highly expressed in wild type and NKCC1-deficient olfactory epithelium. Moreover, we analyzed the transcription of transporters in deficient mice after normalizing to wild type mice Δ CT values to enable the direct comparison of mRNA expression levels. We identified three Slc12 subfamily (Slc12a2/5/9) transporters whose expression significantly decreased in knock-out OE (Fig. 2B). In contrast, we did not detect significant up-regulation of any transporter transcripts in NKCC1-deficient mice.

Signal Transduction Proteins and Western Blotting—Mature olfactory neurons play a major role in odorant recognition due to their ability to convert chemical signals into an electrical cell response (39). Additionally, immature olfactory neurons, like global and horizontal basal cells, contribute to continuous OE regeneration (36, 37). Interestingly, RNA-Seq data revealed that signal transduction-related transcripts decreased in the OE

of NKCC1-deficient mice. We found a significant reduction in the channel subunit Cnga4 expression (wild type/NKCC1-deficient FPKM: 155.3/75), the chloride channel Ano2 (78.3/44) and the phosphodiesterase PDE1C (73.6/40.5). In summary, the NKCC1-deficient mouse OE transcriptome revealed nearly half the transcript number of signal transduction-related genes compared with their wild type littermates (Fig. 3A). We additionally confirmed the RNA-Seq data by RT-PCR experiments (Fig. 3C). We also performed Western blot analysis to verify changes in protein expression between wild type and NKCC1-deficient OE (Fig. 3D). The results validated reduced expression of the olfactory G_{α} subunit, adenylyl cyclase (ACIII), and calmodulin (CaM).

OR Distribution in Wild Type and NKCC1-deficient Mice—OSNs are characterized by their chloride accumulation ability and a dominant expression of mainly one odorant specific G protein-coupled receptor, a so-called olfactory receptor (OR) (39). To date, \sim 900 OR genes have been found to be functional in mice (39–44). RNA-Seq of OE of NKCC1-deficient mice showed that genes involved in the olfactory signal transduction pathway were decreased compared with their wild type littermates. Therefore, we analyzed the olfactory receptor (OR) transcripts found in both mice transcriptomes. RNA-Seq detected the expression of nearly all ORs (wild type: 1060, NKCC1-deficient: 1040) in both transcriptomes (Fig. 4A). Moreover, we found 77 ORs with a FPKM value higher than 10 in wild type OE (Fig. 4B). We performed Cuffdiff analysis to investigate differentially expressed genes in the knock-out OE compared with the wild type OE. We determined that 14% (149 ORs) of the olfactory receptors found in wild type OE were significantly higher ($p < 0.05$) compared with NKCC1-deficient littermates (Fig. 4, C and D). Moreover, 16% of all ORs demonstrated more than a 3-fold higher FPKM value, and 44% of ORs had a 2-fold higher FPKM value in wild type OE (Fig. 4D). In contrast, 19.3% of the annotated ORs in wild type OE displayed higher FPKM values in the NKCC1-deficient transcriptome, whereby only 2.6% had a 2-fold higher FPKM compared with wild type OE. We also verified the reduced expression for two ORs in NKCC1-deficient mice with RT-PCR (Fig. 4E). The reduced FPKM values for 80% of the olfactory receptors are consistent

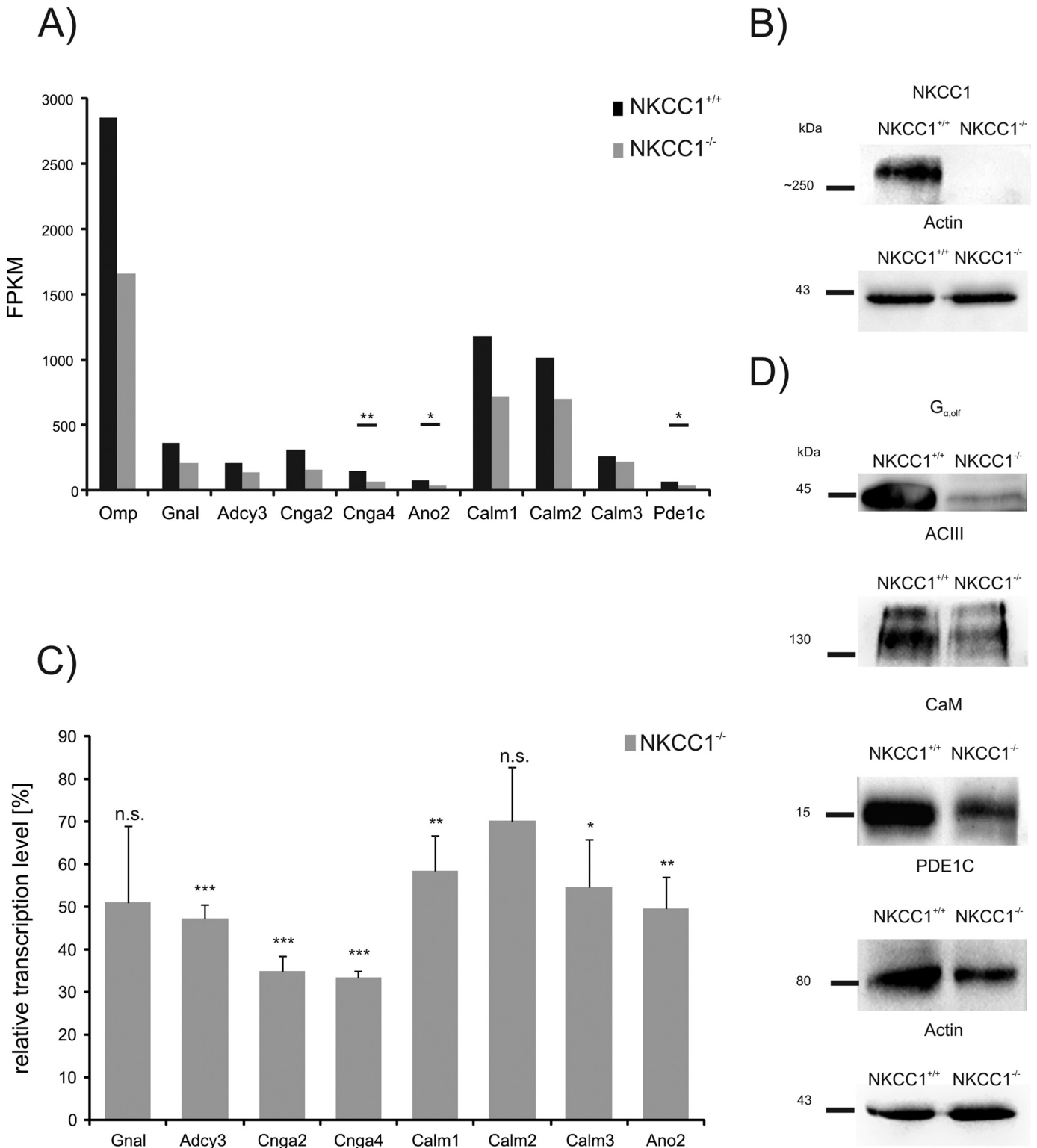


FIGURE 3. A, FPKM values of different olfactory signal transduction proteins and adaptation-associated molecules in both NKCC1-deficient and wild type mice ($n = 3$). B, NKCC1 detection via Western blot analysis of wild type and NKCC1-deficient OE. C, relative transcription level of olfactory signal protein components in NKCC1-deficient mice normalized to wild type transcription level (100%) ($n = 3$). D, Western blot analysis of olfactory G protein, adenylyl cyclase (ACIII), calmodulin (CaM), and β -actin in pooled OE lysate of NKCC1-deficient and wild type mice ($n = 3$).

with the previous findings of lower FPKM values for signal transduction proteins in NKCC1-deficient mice.

Electro-olfactogram Recordings of NKCC1^{-/-} Mice—Olfactory receptor neurons were depolarized in two steps: 1) calcium

and sodium influx, 2) chloride ion efflux, whereby the second step plays the most crucial role for neuronal depolarization. To address whether NKCC1^{-/-} mice have defects in odor perception, we performed air-phase electro-olfactogram recordings

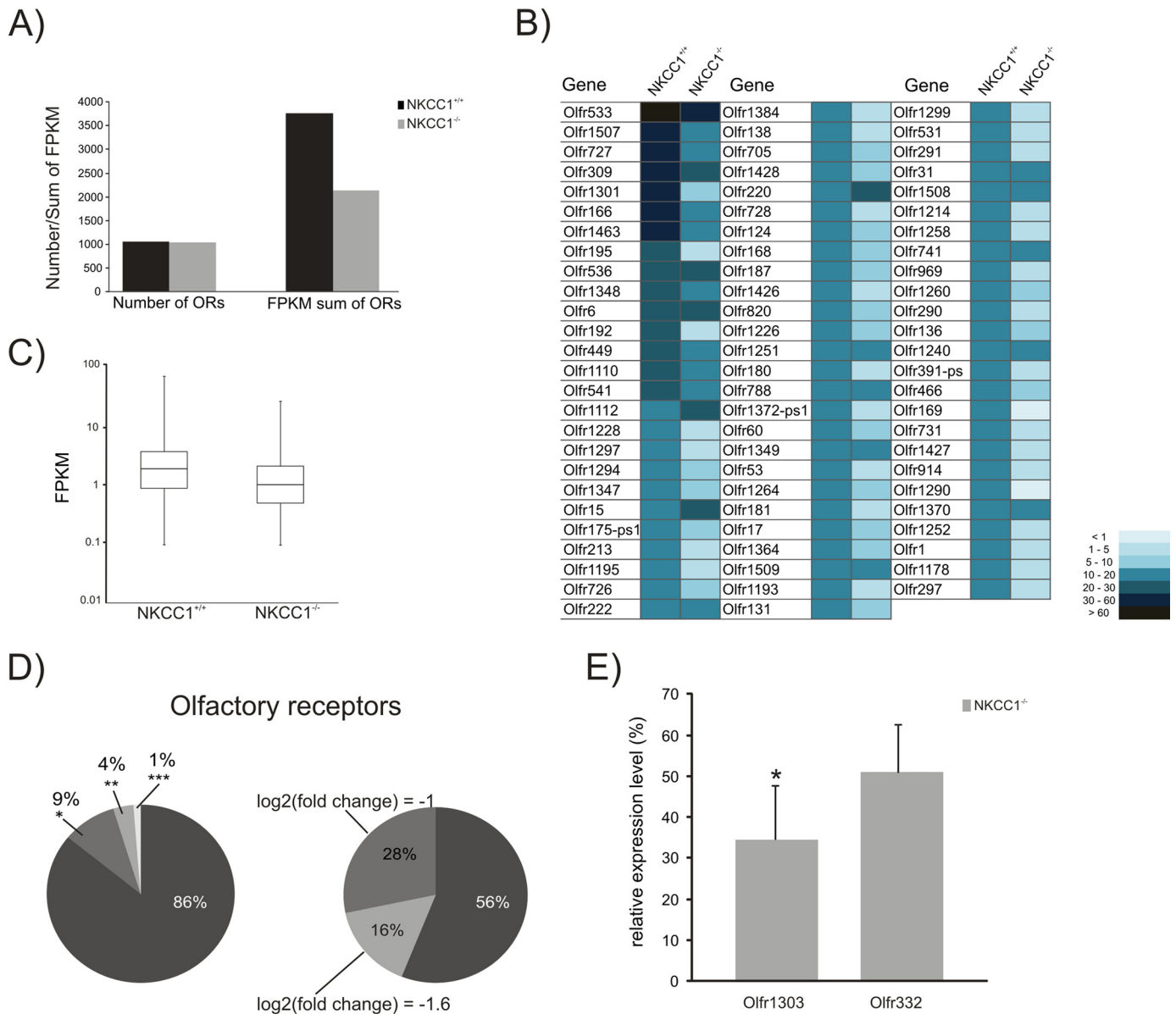


FIGURE 4. Expression analysis of wild type and NKCC1-deficient mice olfactory receptors. A, number of olfactory receptors detected in three different RNA-Seq experiments (FPKM>0.1) and FPKM summation of olfactory receptors of wild type and NKCC1-deficient mice. B, comparison of FPKM values of olfactory receptors with an FPKM>10. C, comparison of FPKM values of ORs. The values of median, upper, and lower quartile are indicated in each box. ORs in wild type are expressed at higher levels compared with NKCC1-deficient mice. D, percentage of significantly lower expressed ORs in NKCC1-deficient mice compared with all ORs in wild type OE and comparison of ORs detected in NKCC1-deficient mice with calculated log₂(fold change) of -1 or -1.6 values compared with wild type (*: $p < 0.05$; **: $p < 0.01$; ***: $p < 0.001$; $n = 3$). E, RT-PCR results of Olfr1303 ($n = 4$) and Olfr332 ($n = 5$) expression in NKCC1-deficient OE compared to wild type OE.

(EOG) with an odorant mixture containing 100 different odorants (Henkel100, dilution 1:1000). This mixture allows for the stimulation of a variety of OSNs (45). The average EOG amplitude in wild type mice was -12.19 ± 1.1 mV, while the average amplitude was -3.04 ± 0.71 mV in NKCC1^{-/-} mice, which is a highly significant ($p < 0.001$) reduction (75%) (Fig. 5, A and E). In addition, the EOG of heterozygous mice exhibited a slight (~18%) but not significant reduction in amplitude (-9.95 ± 1.12 mV, $n = 15$ mice) compared with wild type. The relative rise time was fitted for each odor response, and it was prolonged in NKCC1^{-/-} mice (Fig. 5B). In addition, the NKCC1-deficient mice demonstrated a significant increase (~62%) in the relative decay time ($p < 0.01$) (Fig. 5C). Because of the decreased ampli-

tude, the area under the EOG trace was reduced by ~66% in NKCC1-deficient mice ($p < 0.001$) (Fig. 5D). We also tested the dose dependence of odorant detection for both mice populations using different Henkel100 concentrations. The results showed that for all tested dilutions, wild type mice OE displayed significantly higher amplitudes than NKCC1^{-/-} mice except for the highest dilution tested (1:100,000) (Fig. 6). In summary, NKCC1-deficient mice exhibited a significant decrease in odorant detection also in a dose-dependent manner. As illustrated by the example traces for the generated surface potentials during submerged EOGs, amplitudes were significantly reduced (~85%) in NKCC1-deficient mice (Fig. 7, A and B). In these experiments, we inhibited 50% of the amplitude using niflumic

Ion Transporter Composition of the Murine Olfactory Epithelium

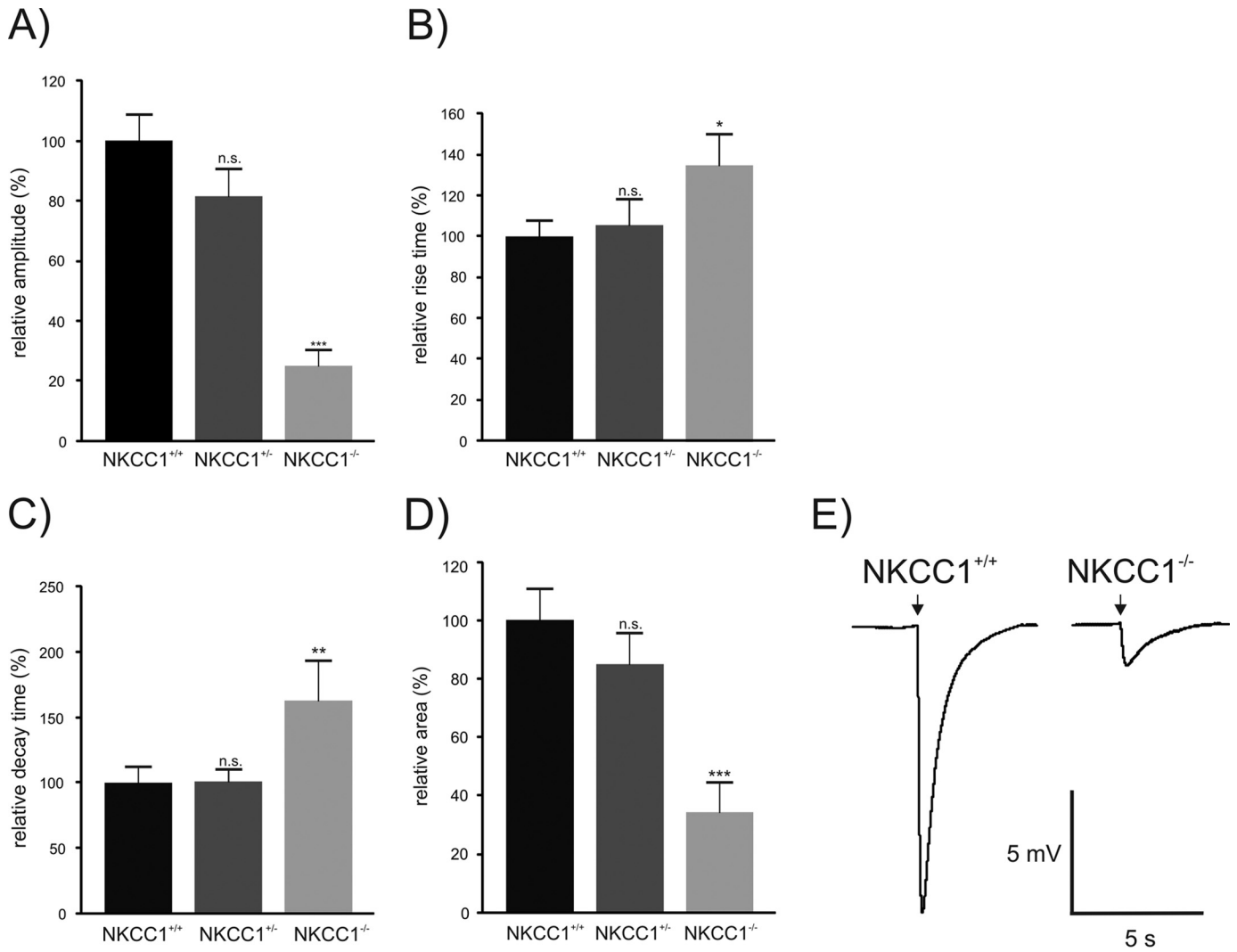


FIGURE 5. **Electro-olfactogram recording analysis of NKCC1^{+/+} (*n* = 18), NKCC1^{+/-} (*n* = 15) and NKCC1^{-/-} mice (*n* = 16, except for relative rise time *n* = 15).** A, normalized amplitude of the measured total surface potential; B, normalized rise time; C, normalized decay time, all normalized to wild type mice; D, normalized area under curve; E, representative EOG traces of NKCC1^{+/+} and NKCC1^{-/-} mice. Arrows indicate 100 ms Henkel100 application.

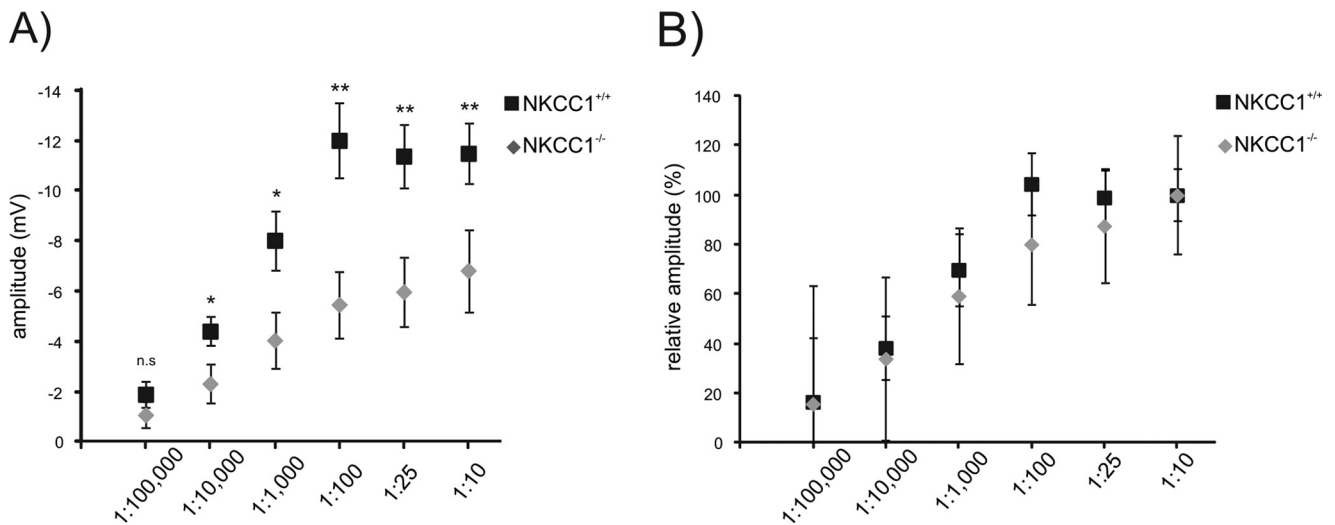


FIGURE 6. **EOG recordings of NKCC1-deficient mice and wild type mice with different Henkel100 dilutions.** (Wild type: *n* = 5, NKCC1^{-/-} mice: *n* = 10).

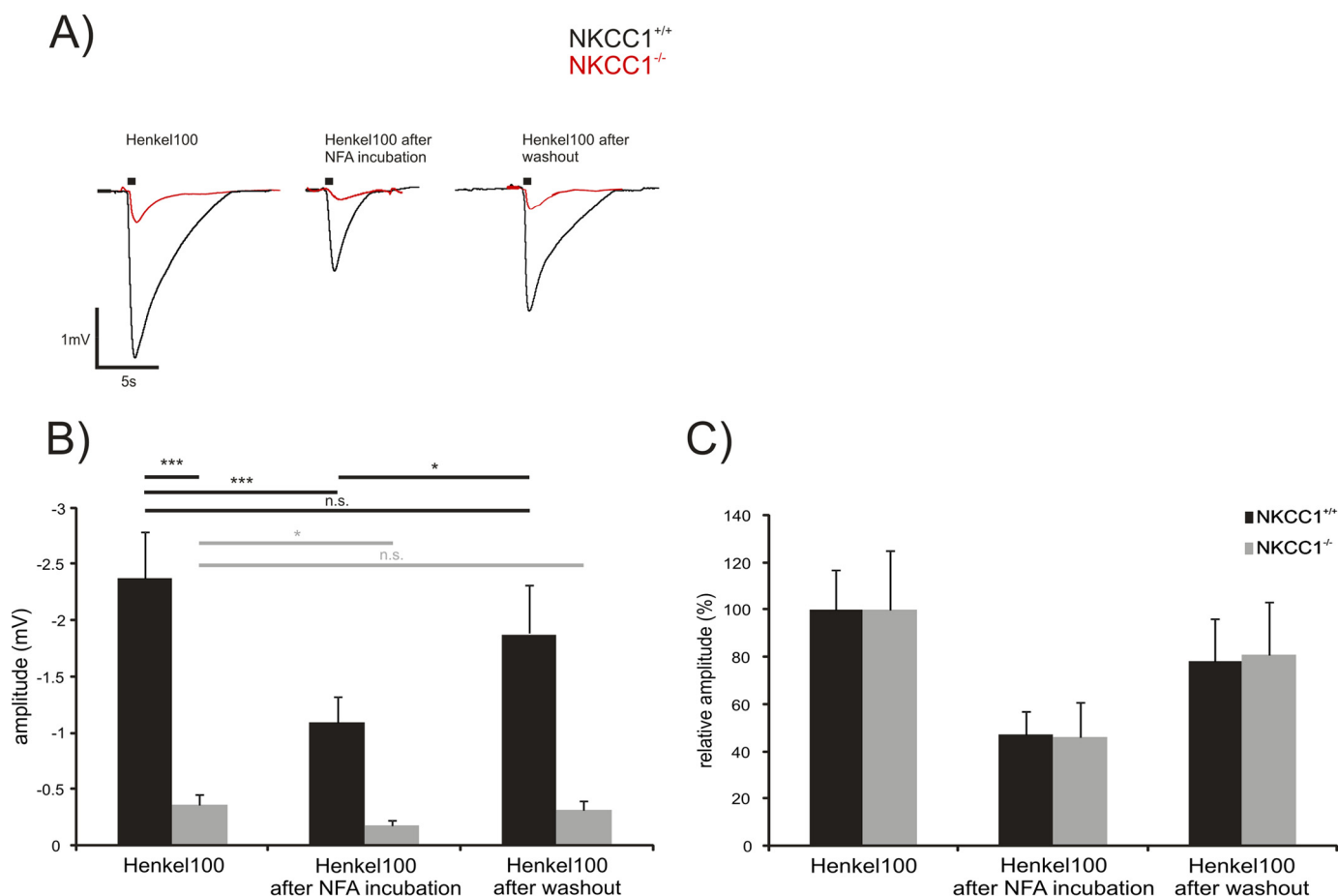


FIGURE 7. **Submerged electro-olfactogram recordings.** *A*, exemplary traces of surface potentials after Henkel100 exposure with and without niflumic acid incubation and washout procedure for wild type ($n = 7$) and $NKCC1$ -KO ($n = 5$) mice. *B*, quantification of mean amplitudes displayed as absolute potentials (mV) and relative potentials (%).

acid, a calcium-activated chloride channel inhibitor (Fig. 7C). Subsequent niflumic acid washout led to ~80% signal recovery (46). Interestingly, niflumic acid had the same effect on $NKCC1$ -deficient as wild type OE. This effect was previously described by Nickell *et al.* (2007), suggesting that the measured surface potentials rely on the same proportion of chloride efflux as the amplitudes generated by wild type littermates.

Neuronal Layer Thickness and Cell Number—Our electrophysiological experiments revealed a significant impact of $NKCC1$ in both air-phase and submerged EOGs. Submerged EOG also demonstrated that the generated surface potentials rely on the same proportion of chloride efflux in both wild type and $NKCC1$ -deficient mice. These results suggest that $NKCC1$ -deficient OE still maintains functional chloride accumulation due to another chloride transporter. These findings combined with the RNA-Seq results led us to the hypothesis that $NKCC1$ -deficient mice exhibit a decreased number of olfactory neurons compared with wild type littermates. Because of $NKCC1$'s known role in brain plasticity and its known function in cell homeostasis (47), we examined changes in $NKCC1^{-/-}$ OE morphology. We measured turbinate length but found no significant difference between wild type and $NKCC1$ -deficient populations (data not shown). We also performed hematoxylin/eosin staining of coronal cryosections and measured the neuronal layer thickness in the OE of wild type

and $NKCC1$ -deficient mice. Here, we measured a significant 20% decrease in neuronal layer thickness for $NKCC1$ -deficient mice (Fig. 8A). We additionally stained OE cryosections with DAPI for visualizing the cell nucleus and counted the cells in the neuronal layer of the epithelium (Fig. 8B). Analyses of wild type, heterozygous and $NKCC1$ -deficient cryosections revealed 20% less cells in OE lacking $NKCC1$ compared with wild type OE. There was no difference in cell number between wild type and heterozygous OE. In conclusion, the reduced neuronal layer thickness is due to a decrease in cell number in the OE of $NKCC1$ -deficient mice.

DISCUSSION

In this study, we demonstrated that the ion transporter $NKCC1$ is not only responsible for chloride accumulation, but it is also involved in the continuous neurogenesis of the murine OE. The impact of $NKCC1$ on chloride accumulation in OSNs has been controversially discussed for several years. To overcome this controversy and to uncover the role of $NKCC1$, we generated RNA-Seq transcriptome data of $NKCC1$ -deficient and wild type mice to monitor OE gene expression.

Focusing on chloride-related transporters, our RNA-Seq data revealed a high number of mRNA transcripts for a Na^+ - and Cl^- -dependent taurin transporter (*Slc6a6*) in both wild type and $NKCC1$ -deficient mice. *Slc6a6* encodes a neurotrans-

Ion Transporter Composition of the Murine Olfactory Epithelium

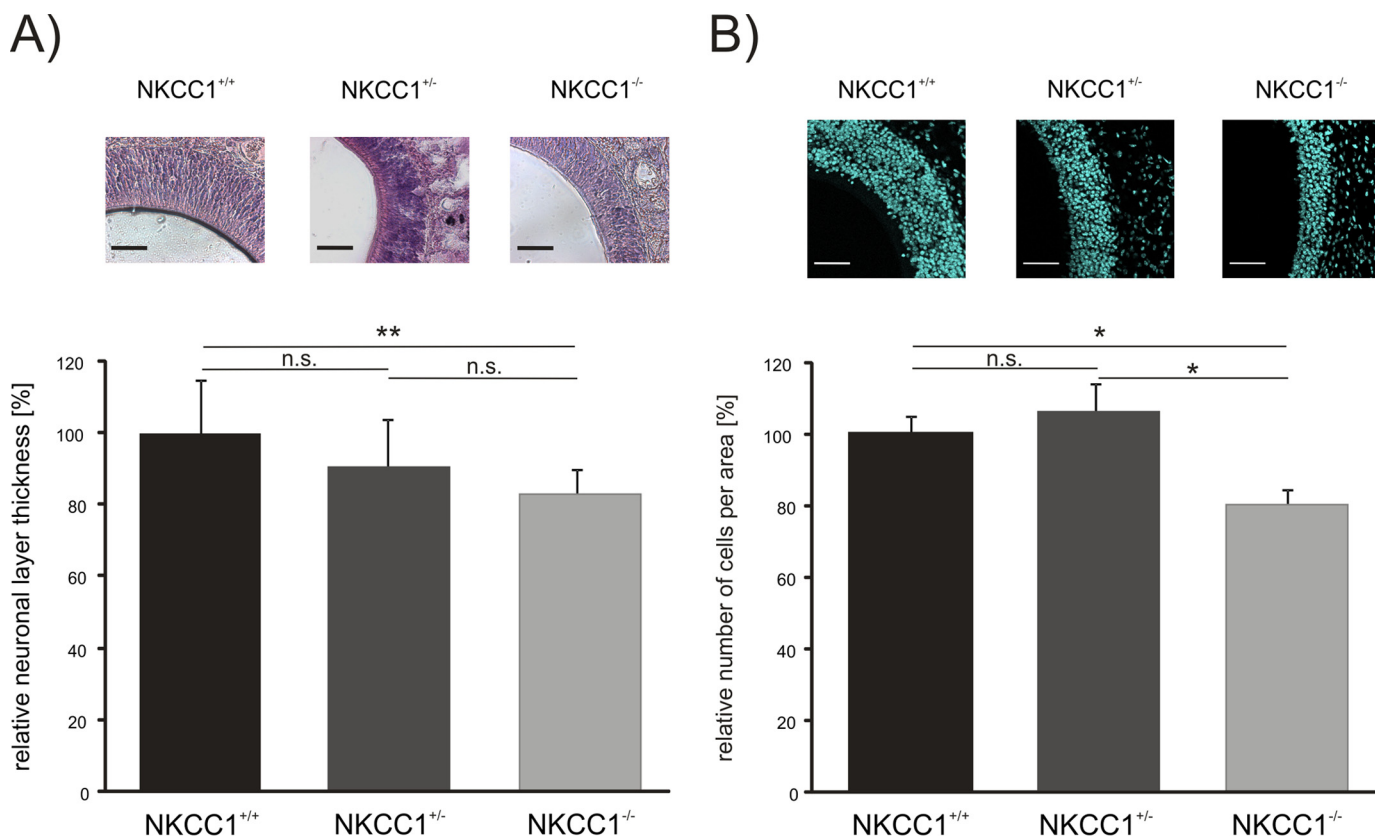


FIGURE 8. **Morphological changes of NKCC1-deficient mice OE.** A, olfactory neuronal layer thickness is decreased in heterozygous and NKCC1-deficient mice compared with wild type mice. (*NKCC1*^{+/+}: *n* = 10, *NKCC1*^{+/-}: *n* = 13, *NKCC1*^{-/-}: *n* = 10). B, relative number of cells is decreased in NKCC1-deficient OE (*NKCC1*^{+/+}: *n* = 10, *NKCC1*^{+/-}: *n* = 11, *NKCC1*^{-/-}: *n* = 12) (**: *p* < 0.01; *: *p* < 0.05). Scale bar 50 μ m.

mitter transporter that carries β -amino acids and taurine to the neuronal apical membrane. Chloride ions are essential for optimal taurin uptake by the transporter whereby chloride influx is coupled to an efflux mediated by another transporter such that the net stoichiometry is 1 Taurin: 2 Na^+ -ions (48–50). Furthermore, RNA-Seq data from isolated neurons displayed decreased *Slc6a6* mRNA transcript levels compared with whole OE (34). This suggests that the taurin transporter is predominantly expressed in other OE cell types than neurons. Thus, the involvement of *Slc6a6* in olfactory neuron chloride accumulation is unlikely. The electroneutral chloride transporter NKCC1 was the second highest expressed *Slc*-transporter in the OE and the highest in FACS-sorted OSNs (34). These findings explain NKCC1's chloride accumulation function during suction-pipette measurements of isolated neurons (16). The third highest expressed ion transporter in the OE was the DIDS-sensitive $\text{Cl}^-/\text{HCO}_3^-$ -exchanger *Slc26a7*. This transporter is thought to accumulate chloride ions in different cell types (51, 52). In contrast, when expressed in *Xenopus laevis* oocytes or HEK293 cells, human *SLC26A7* functions as a pH_i -regulated Cl^- -channel with minimal $\text{OH}^-/\text{HCO}_3^-$ -permeability (53). Therefore, its function in OSNs remains unclear. The second anion exchanger *Slc4a2* (AE2) detected via RNA-seq is a presumed chloride accumulator in olfactory neurons (54). Nonetheless, Nickell and coworkers previously investigated AE2's effect on chloride accumulation in olfactory neurons (17). Their EOG measurements of an AE2 knock-out mouse revealed that the ion exchanger has no impact on chloride accu-

mulation and thus no effect on odorant detection. The RNA-Seq results demonstrated a slightly higher FPKM value for *Slc4a2* in the NKCC1-deficient transcriptome, while RT-PCR revealed that there was no significant increase in transcription of this chloride transporter gene. Nevertheless, if a transporter is primarily expressed in OSNs and the number of OSNs is reduced in NKCC1-deficient mice, both the RNA-Seq data and RT-PCR data should display reduced expression of this transporter. Indeed, RT-PCR demonstrated a significant decrease in *Slc12a9* expression, which is more highly expressed in OSN than in OE, *Slc12a2*, a highly expressed transporter in OSN, and neuron-specific *Slc12a5*. Thus, the decrease in transporter expression can be explained by the reduced OSN number in NKCC1-deficient mice. These results also imply that transporter *Slc4a3*, *Slc26a7*, *Slc4a2*, *Slc12a7*, and *Slc12a6* expression is enhanced compared with wild type mice. The *Slc4a3*, *Slc26a7*, and *Slc4a2* transporters are possible chloride accumulators in the OSN. However, only *Slc26a7* is a likely chloride accumulator candidate beside NKCC1, as *Slc4a2* knock-out mice have no defects in odorant perception in EOG (17), and *Slc4a3* showed low expression in both RNA-Seq and RT-PCR experiments. In summary, RNA-Seq analysis demonstrated that NKCC1 is the most highly expressed chloride transporter in both OE and OSN, and the transporter *Slc26a7* may also be involved in chloride accumulation.

RNA-Seq analysis of wild type and NKCC1-deficient transcriptomes demonstrated a reduction in mRNA of signaling pathway-related genes and olfactory receptors. Cuffdiff analysis

revealed a significant mRNA decrease of the calcium channel subunit 4 (Cnga4), the chloride channel Ano2 and the phosphodiesterase PDE1C. Additionally, statistics revealed that 14% of ORs in NKCC1 knock-out mice exhibited significantly reduced FPKM values for these receptor genes. Calculation of the FPKM ratios of wild type and NKCC1-deficient mice for signal transduction-related and OR genes revealed an average ratio of 1.68 ± 0.25 and 4.76 ± 2.56 , respectively. The ratio indicates an ~ 2 -fold change in expression of signal transduction-related genes. The average FPKM ratio for OR genes demonstrates that ORs display higher FPKM values in wild type mice, but these values had large ranges. RT-PCR experiments additionally validated the reduction of signaling pathway genes and olfactory receptors. For the first time, these results implied decreased transcription of these genes, resulting in lower OSN sensitivity or reduced neuron number in NKCC1-deficient mice.

The Cuffdiff analysis of RNA-Seq experiments revealed 45 genes with a significant regulation in NKCC1-deficient mice (data not shown). We identified 6 olfactory receptors with significantly lower FPKM values in NKCC1-deficient mice. These findings support our analysis in which we identified 149 ORs ($p < 0.05$) that had notably decreased expression in NKCC1-deficient mice. Focusing on ion-related proteins, we recognized two Slc-transporters, the urea transporter Slc14a2 (55) and the sodium/potassium/calcium Exchanger 2 (Slc24a2) (56) that had reduced expression in NKCC1-deficient mice. The Slc24a2 transporter functions as a calcium extruder in neurons (57). Therefore, its down-regulation impairs calcium transport and could negatively influence the excitability of the NKCC1-deficient neurons. We also identified a calcium-activated potassium channel (Kcnmb3) involved in neuronal excitability (58, 59) and a channel-associated protein (Dlg2) that acts as a scaffolding protein in neurons (60) that had increased expression in wild type OE. Dlg2 is involved in mitotic cell organization in neuronal synapses in *Drosophila melanogaster* (61, 62). Consequently, the decreased Dlg2 expression in NKCC1-deficient mice might negatively influence OE neurogenesis. We additionally identified genes with higher expression levels in knock-out compared with wild type mice. A calcium-activated chloride channel (Clca2) (63) exhibited a higher FPKM value in the NKCC1-deficient transcriptome. This chloride channel is expressed in a subset of OSNs and may play a role in odorant transduction in cilia (64). Moreover, protocadherin 10 (Pcdh10), a gene with key roles in suppressing cell proliferation (65), displayed a higher FPKM value in NKCC1-deficient mice. Therefore, Pcdh10 overexpression might contribute to the neurogenesis defects in the NKCC1-deficient OE. We also identified the transient receptor potential channel melastatin 5 (Trpm5) and two claudins (Cldn2, Cldn4) that were more highly expressed in deficient OE. Trpm5 channels mediate pheromone transduction in the OE (66), and claudins are tight junction components that maintain the cellular polarity (67). In summary, we identified several ion-/development-related genes with modified expression levels in NKCC1-deficient mice that may contribute to the impaired odorant transduction and/or OE development.

The electro-olfactogram recordings demonstrated that NKCC1 affects surface potentials, confirmed by the highly sig-

nificant decrease ($\sim 75\%$) in surface amplitudes generated by NKCC1-deficient mice. We also measured surface potentials with different Henkel100 dilutions and generated amplitudes with an overall significant decrease in deficient mice. The results also displayed the same concentration dependence for generated surface potentials and the achievement of the maximal amplitude in both approaches. These findings exclude the hypothesis that NKCC1 loss induces olfactory neuron insensitivity. Submerged EOGs displayed reduced amplitudes and implied insufficient odorant recognition in NKCC1-deficient mice. In contrast, the inhibition of calcium-gated chloride channels demonstrated that OSN depolarization of both mouse populations relies on the same proportion of the chloride efflux. This effect was previously described by Nickell and coworkers using EOG recordings (17). Although they measured a minor 57% reduction in amplitudes of NKCC1^{-/-} mice (18), we observed a $\sim 75\%$ decrease in amplitudes in knock-out mice. These differences in amplitude are likely due to slightly different application systems and different aged mice (NKCC1^{+/+}: 109 ± 4 days, NKCC1^{-/-}: 109 ± 3 , Nickell: NKCC1^{+/+}: 87 ± 5 days, NKCC1^{-/-}: 111 ± 11 days), resulting in strong signal amplitudes (NKCC1^{+/+}: ~ 12 mV, NKCC1^{-/-}: ~ 3 mV), which was also reported by Nickell (17). In 2006, he presumed a 39% amplitude reduction in NKCC1 knock-out mice, and conversely, he reported a 57% decrease in 2007 due to the age of mice and technique. The finding that the lack of NKCC1 has no impact on the proportion of chloride efflux in olfactory neurons is in contrast to the large amplitude reduction measured during EOG experiments. Electrophysiological and RNA-Seq experiments suggest that: (i) NKCC1-deficient OSNs actively accumulate chloride ions via an unidentified ion transporter and/or (ii) the OE contains less mature neurons than wild type OE.

The measurements of neuronal layer thickness and cell number of wild type, heterozygous, and NKCC1 knock-out mice revealed a decrease of $\sim 20\%$ in both thickness and cell number in the NKCC1-deficient mice. These findings were supported by both the RNA-Seq and RT-PCR results. In summary, the lack of NKCC1 leads to a reduced number of mature neurons due to an inhibition of cell proliferation. NKCC1 is a well-known cell cycle regulator in cultured cell lines (20, 21). In addition, previous studies suggested a role of NKCC1 in regeneration after nerve injuries and postnatal neurogenesis in the brain (23, 25). The association of our results and previous studies suggest that NKCC1 is involved in continuous OE neurogenesis. This study reveals a new aspect of NKCC1 loss and its consequences for odorant sensation in mice. It also attempts to explain the different results regarding the impact of NKCC1 in olfaction obtained by several researchers over the years. Nevertheless, further investigations will focus on the molecular mechanism of NKCC1 in adult OE neurogenesis.

Acknowledgments—We thank Prof. Dr. med. Ursula Seidler (Hanover Medical School) for the donation of NKCC1 knock-out mice. We also thank Simon Pyschny, Fabian Jansen, and Benjamin Kalbe for a great support during electro-olfactogram recordings and helpful discussion input.

REFERENCES

- Bakalyar, H. A., and Reed, R. R. (1990) Identification of a specialized adenylyl cyclase that may mediate odorant detection. *Science* **250**, 1403–1406
- Lowe, G., Nakamura, T., and Gold, G. H. (1989) Adenylate cyclase mediates olfactory transduction for a wide variety of odorants. *Proc. Natl. Acad. Sci. U.S.A.* **86**, 5641–5645
- Nakamura, T., and Gold, G. H. (1987) A cyclic nucleotide-gated conductance in olfactory receptor cilia. *Nature* **325**, 442–444
- Billig, G. M., Pál, B., Fidzinski, P., and Jentsch, T. J. (2011) Ca²⁺-activated Cl⁻ currents are dispensable for olfaction. *Nat. Neurosci.* **14**, 763–769
- Stephan, A. B., Shum, E. Y., Hirsh, S., Cygnar, K. D., Reisert, J., and Zhao, H. (2009) ANO2 is the ciliary calcium-activated chloride channel that may mediate olfactory amplification. *Proc. Natl. Acad. Sci. U.S.A.* **106**, 11776–11781
- Rasche, S., Toetter, B., Adler, J., Tschapek, A., Doerner, J. F., Kurtenbach, S., Hatt, H., Meyer, H., Warscheid, B., and Neuhaus, E. M. (2010) Tmem16b is specifically expressed in the cilia of olfactory sensory neurons. *Chem. Senses* **35**, 239–245
- Lowe, G., and Gold, G. H. (1993) Nonlinear amplification by calcium-dependent chloride channels in olfactory receptor cells. *Nature* **366**, 283–286
- Kaplan, M. R., Plotkin, M. D., Brown, D., Hebert, S. C., and Delpire, E. (1996) Expression of the mouse Na-K-2Cl cotransporter, mBSC2, in the terminal inner medullary collecting duct, the glomerular and extraglomerular mesangium, and the glomerular afferent arteriole. *J. Clin. Invest.* **98**, 723–730
- Bouyer, P. G., Tang, X., Weber, C. R., Shen, L., Turner, J. R., and Matthews, J. B. (2013) Capsaicin induces NKCC1 internalization and inhibits chloride secretion in colonic epithelial cells independently of TRPV1. *Am. J. Physiol. Gastrointest Liver Physiol* **304**, G142–156
- Chen, H., and Sun, D. (2005) The role of Na-K-Cl co-transporter in cerebral ischemia. *Neurol. Res.* **27**, 280–286
- Kakigi, A., Nishimura, M., Takeda, T., Taguchi, D., and Nishioka, R. (2009) Expression of aquaporin1, 3, and 4, NKCC1, and NKCC2 in the human endolymphatic sac. *Auris Nasus Larynx* **36**, 135–139
- Schöbel, N., Radtke, D., Lübbert, M., Gisselmann, G., Lehmann, R., Cichy, A., Schreiner, B. S., Altmüller, J., Spector, A. C., Spehr, J., Hatt, H., and Wetzel, C. H. (2012) Trigeminal ganglion neurons of mice show intracellular chloride accumulation and chloride-dependent amplification of capsaicin-induced responses. *PLoS One* **7**, e48005
- Liu, Q., and Wong-Riley, M. T. (2012) Postnatal development of Na(+)-K(+)-2Cl(-) co-transporter 1 and K(+)-Cl(-) co-transporter 2 immunoreactivity in multiple brain stem respiratory nuclei of the rat. *Neuroscience* **210**, 1–20
- Clarkson, A. N., Huang, B. S., Macisaac, S. E., Mody, I., and Carmichael, S. T. (2010) Reducing excessive GABA-mediated tonic inhibition promotes functional recovery after stroke. *Nature* **468**, 305–309
- Karpova, N. N., Pickenhagen, A., Lindholm, J., Tiraboschi, E., Kuleskaya, N., Agústsdóttir, A., Antila, H., Popova, D., Akamine, Y., Bahi, A., Sullivan, R., Hen, R., Drew, L. J., and Castrén, E. (2011) Fear erasure in mice requires synergy between antidepressant drugs and extinction training. *Science* **334**, 1731–1734
- Reisert, J., Lai, J., Yau, K. W., and Bradley, J. (2005) Mechanism of the excitatory Cl⁻ response in mouse olfactory receptor neurons. *Neuron* **45**, 553–561
- Nickell, W. T., Kleene, N. K., and Kleene, S. J. (2007) Mechanisms of neuronal chloride accumulation in intact mouse olfactory epithelium. *J. Physiol.* **583**, 1005–1020
- Nickell, W. T., Kleene, N. K., Gesteland, R. C., and Kleene, S. J. (2006) Neuronal chloride accumulation in olfactory epithelium of mice lacking NKCC1. *J. Neurophysiol.* **95**, 2003–2006
- Smith, D. W., Thach, S., Marshall, E. L., Mendoza, M. G., and Kleene, S. J. (2008) Mice lacking NKCC1 have normal olfactory sensitivity. *Physiol. Behav.* **93**, 44–49
- Panet, R., Eliash, M., Pick, M., and Atlan, H. (2002) Na(+)/K(+)/Cl(-) cotransporter activates mitogen-activated protein kinase in fibroblasts and lymphocytes. *J. Cell. Physiol.* **190**, 227–237
- Panet, R., Marcus, M., and Atlan, H. (2000) Overexpression of the Na(+)/K(+)/Cl(-) cotransporter gene induces cell proliferation and phenotypic transformation in mouse fibroblasts. *J. Cell. Physiol.* **182**, 109–118
- Nakajima, K., Miyazaki, H., Niisato, N., and Marunaka, Y. (2007) Essential role of NKCC1 in NGF-induced neurite outgrowth. *Biochem. Biophys. Res. Commun.* **359**, 604–610
- Pieraut, S., Laurent-Matha, V., Sar, C., Hubert, T., Méchaly, I., Hilaire, C., Mersel, M., Delpire, E., Valmier, J., and Scamps, F. (2007) NKCC1 phosphorylation stimulates neurite growth of injured adult sensory neurons. *J. Neurosci.* **27**, 6751–6759
- Lu, K. T., Huang, T. C., Wang, J. Y., You, Y. S., Chou, J. L., Chan, M. W., Wo, P. Y., Amstislavskaya, T. G., Tikhonova, M. A., and Yang, Y. L. (2014) NKCC1 mediates traumatic brain injury-induced hippocampal neurogenesis through CREB phosphorylation and HIF-1α expression. *Pflugers Arch.*
- Sun, L., Yu, Z., Wang, W., and Liu, X. (2012) Both NKCC1 and anion exchangers contribute to Cl⁻ accumulation in postnatal forebrain neuronal progenitors. *Eur. J. Neurosci.* **35**, 661–672
- Flagella, M., Clarke, L. L., Miller, M. L., Erway, L. C., Giannella, R. A., Andringa, A., Gawenis, L. R., Kramer, J., Duffy, J. J., Doetschman, T., Lorenz, J. N., Yamoah, E. N., Cardell, E. L., and Shull, G. E. (1999) Mice lacking the basolateral Na-K-2Cl cotransporter have impaired epithelial chloride secretion and are profoundly deaf. *J. Biol. Chem.* **274**, 26946–26955
- Trapnell, C., Roberts, A., Goff, L., Pertea, G., Kim, D., Kelley, D. R., Pimentel, H., Salzberg, S. L., Rinn, J. L., and Pachter, L. (2012) Differential gene and transcript expression analysis of RNA-seq experiments with TopHat and Cufflinks. *Nat. Protoc.* **7**, 562–578
- Trapnell, C., Pachter, L., and Salzberg, S. L. (2009) TopHat: discovering splice junctions with RNA-Seq. *Bioinformatics* **25**, 1105–1111
- Langmead, B., Trapnell, C., Pop, M., and Salzberg, S. L. (2009) Ultrafast and memory-efficient alignment of short DNA sequences to the human genome. *Genome Biol.* **10**, R25
- Li, H., Handsaker, B., Wysoker, A., Fennell, T., Ruan, J., Homer, N., Marth, G., Abecasis, G., and Durbin, R. (2009) The Sequence Alignment/Map format and SAMtools. *Bioinformatics* **25**, 2078–2079
- Trapnell, C., Williams, B. A., Pertea, G., Mortazavi, A., Kwan, G., van Baren, M. J., Salzberg, S. L., Wold, B. J., and Pachter, L. (2010) Transcript assembly and quantification by RNA-Seq reveals unannotated transcripts and isoform switching during cell differentiation. *Nat. Biotechnol.* **28**, 511–515
- Roberts, A., Trapnell, C., Donaghey, J., Rinn, J. L., and Pachter, L. (2011) Improving RNA-Seq expression estimates by correcting for fragment bias. *Genome Biol.* **12**, R22
- Kurtenbach, S., Wewering, S., Hatt, H., Neuhaus, E. M., and Lübbert, H. (2013) Olfaction in three genetic and two MPTP-induced Parkinson's disease mouse models. *PLoS One* **8**, e77509
- Kanageswaran, N., Demond, M., Nagel, M., Schreiner, B. S., Baumgart, S., Scholz, P., Altmüller, J., Becker, C., Doerner, J. F., Conrad, H., Oberland, S., Wetzel, C. H., Neuhaus, E. M., Hatt, H., and Gisselmann, G. (2015) Deep Sequencing of the Murine Olfactory Receptor Neuron Transcriptome. *PLoS One* **10**, e0113170
- Schneider, C. A., Rasband, W. S., and Eliceiri, K. W. (2012) NIH Image to ImageJ: 25 years of image analysis. *Nat. Methods* **9**, 671–675
- Graziadei, P. P., and Graziadei, G. A. (1979) Neurogenesis and neuron regeneration in the olfactory system of mammals. I. Morphological aspects of differentiation and structural organization of the olfactory sensory neurons. *J. Neurocytol.* **8**, 1–18
- Huard, J. M., Youngentob, S. L., Goldstein, B. J., Luskin, M. B., and Schwob, J. E. (1998) Adult olfactory epithelium contains multipotent progenitors that give rise to neurons and non-neural cells. *J. Comp. Neurol.* **400**, 469–486
- Potter, S. M., Zheng, C., Koos, D. S., Feinstein, P., Fraser, S. E., and Mombaerts, P. (2001) Structure and emergence of specific olfactory glomeruli in the mouse. *J. Neurosci.* **21**, 9713–9723
- Buck, L., and Axel, R. (1991) A novel multigene family may encode odorant receptors: a molecular basis for odor recognition. *Cell* **65**, 175–187

40. Godfrey, P. A., Malnic, B., and Buck, L. B. (2004) The mouse olfactory receptor gene family. *Proc. Natl. Acad. Sci. U.S.A.* **101**, 2156–2161
41. Mombaerts, P. (2004) Odorant receptor gene choice in olfactory sensory neurons: the one receptor-one neuron hypothesis revisited. *Curr. Opin. Neurobiol.* **14**, 31–36
42. Glusman, G., Yanai, I., Rubin, I., and Lancet, D. (2001) The complete human olfactory subgenome. *Genome Res.* **11**, 685–702
43. Niimura, Y., and Nei, M. (2007) Extensive gains and losses of olfactory receptor genes in mammalian evolution. *PLoS One* **2**, e708
44. DeMaria, S., and Ngai, J. (2010) The cell biology of smell. *J. Cell Biol.* **191**, 443–452
45. Spehr, M., Wetzel, C. H., Hatt, H., and Ache, B. W. (2002) 3-phosphoinositides modulate cyclic nucleotide signaling in olfactory receptor neurons. *Neuron* **33**, 731–739
46. Lerma, J., and Martín del Río, R. (1992) Chloride transport blockers prevent N-methyl-D-aspartate receptor-channel complex activation. *Mol. Pharmacol.* **41**, 217–222
47. Ikeda, M., Toyoda, H., Yamada, J., Okabe, A., Sato, K., Hotta, Y., and Fukuda, A. (2003) Differential development of cation-chloride cotransporters and Cl⁻ homeostasis contributes to differential GABAergic actions between developing rat visual cortex and dorsal lateral geniculate nucleus. *Brain Res.* **984**, 149–159
48. Ramamoorthy, S., Leibach, F. H., Mahesh, V. B., Han, H., Yang-Feng, T., Blakely, R. D., and Ganapathy, V. (1994) Functional characterization and chromosomal localization of a cloned taurine transporter from human placenta. *Biochem. J.* **300**, 893–900
49. Loo, D. D., Eskandari, S., Boorer, K. J., Sarkar, H. K., and Wright, E. M. (2000) Role of Cl⁻ in electrogenic Na⁺-coupled cotransporters GAT1 and SGLT1. *J. Biol. Chem.* **275**, 37414–37422
50. Bicho, A., and Grewer, C. (2005) Rapid substrate-induced charge movements of the GABA transporter GAT1. *Biophys. J.* **89**, 211–231
51. Petrovic, S., Ju, X., Barone, S., Seidler, U., Alper, S. L., Lohi, H., Kere, J., and Soleimani, M. (2003) Identification of a basolateral Cl⁻/HCO₃⁻ exchanger specific to gastric parietal cells. *Am. J. Physiol. Gastrointest Liver Physiol.* **284**, G1093–G1103
52. Kosiek, O., Busque, S. M., Föller, M., Shcheynikov, N., Kirchhoff, P., Bleich, M., Muallem, S., and Geibel, J. P. (2007) SLC26A7 can function as a chloride-loading mechanism in parietal cells. *Pflugers Arch* **454**, 989–998
53. Kim, K. H., Shcheynikov, N., Wang, Y., and Muallem, S. (2005) SLC26A7 is a Cl⁻ channel regulated by intracellular pH. *J. Biol. Chem.* **280**, 6463–6470
54. Kurschat, C. E., Shmukler, B. E., Jiang, L., Hevi, S., Kim, E. H., Stewart, A. K., and Alper, S. L. (2008) Mouse strain-specific coding polymorphism in the Slc4a2/Ae2 gene encodes Ae2c2 variants differing in isoform-specific dominant negative activity. *Exp. Physiol.* **93**, 458–467
55. Fenton, R. A., Cottingham, C. A., Stewart, G. S., Howorth, A., Hewitt, J. A., and Smith, C. P. (2002) Structure and characterization of the mouse UT-A gene (Slc14a2). *Am. J. Physiol. Renal Physiol.* **282**, F630–638
56. Li, X. F., Kraev, A. S., and Lytton, J. (2002) Molecular cloning of a fourth member of the potassium-dependent sodium-calcium exchanger gene family, NCKX4. *J. Biol. Chem.* **277**, 48410–48417
57. Altimimi, H. F., and Schnetkamp, P. P. (2007) Na⁺-dependent inactivation of the retinal cone/brain Na⁺/Ca²⁺-K⁺ exchanger NCKX2. *J. Biol. Chem.* **282**, 3720–3729
58. Behrens, R., Nolting, A., Reimann, F., Schwarz, M., Waldschütz, R., and Pongs, O. (2000) hKCNMB3 and hKCNMB4, cloning and characterization of two members of the large-conductance calcium-activated potassium channel beta subunit family. *FEBS Lett.* **474**, 99–106
59. Hu, S., Labuda, M. Z., Pandolfo, M., Goss, G. G., McDermid, H. E., and Ali, D. W. (2003) Variants of the KCNMB3 regulatory subunit of maxi BK channels affect channel inactivation. *Physiol. Genomics* **15**, 191–198
60. Roberts, S., Delury, C., and Marsh, E. (2012) The PDZ protein discs-large (DLG): the 'Jekyll and Hyde' of the epithelial polarity proteins. *FEBS J.* **279**, 3549–3558
61. Albertson, R., and Doe, C. Q. (2003) Dlg, Scrib and Lgl regulate neuroblast cell size and mitotic spindle asymmetry. *Nat. Cell Biol.* **5**, 166–170
62. Goode, S., and Perrimon, N. (1997) Inhibition of patterned cell shape change and cell invasion by Discs large during *Drosophila* oogenesis. *Genes Dev.* **11**, 2532–2544
63. Piirsoo, M., Meijer, D., and Timmusk, T. (2009) Expression analysis of the CLCA gene family in mouse and human with emphasis on the nervous system. *BMC Dev. Biol.* **9**, 10
64. Gonzalez-Silva, C., Vera, J., Bono, M. R., González-Billault, C., Baxter, B., Hansen, A., Lopez, R., Gibson, E. A., Restrepo, D., and Bacigalupo, J. (2013) Ca²⁺-activated Cl⁻ channels of the ClCa family express in the cilia of a subset of rat olfactory sensory neurons. *PLoS One* **8**, e69295
65. Zhong, X., Zhu, Y., Mao, J., Zhang, J., and Zheng, S. (2013) Frequent epigenetic silencing of PCDH10 by methylation in human colorectal cancer. *J. Cancer Res. Clin. Oncol.* **139**, 485–490
66. López, F., Delgado, R., López, R., Bacigalupo, J., and Restrepo, D. (2014) Transduction for pheromones in the main olfactory epithelium is mediated by the Ca²⁺-activated channel TRPM5. *J. Neurosci.* **34**, 3268–3278
67. Morita, K., Furuse, M., Fujimoto, K., and Tsukita, S. (1999) Claudin multigene family encoding four-transmembrane domain protein components of tight junction strands. *Proc. Natl. Acad. Sci. U.S.A.* **96**, 511–516